ELSEVIER

Chemical Engineering Journal 90 (2002) 77–87

Chemical Engineering Journal

www.elsevier.com/locate/cej

Quantitative investigation of catalytic natural gas conversion for hydrogen fuel cell applications

Ahmet K. Avcı [a], David L. Trimm [b], Z. Ilsen Önsan [a,*]

[a] *Department of Chemical Engineering, Boğaziçi University, 80815 Bebek, Istanbul, Turkey*
[b] *School of Chemical Engineering and Industrial Chemistry, University of New South Wales, Sydney 2052, Australia*

Abstract

Hydrogen generation from natural gas for driving proton exchange membrane fuel cells in residential small-scale combined heat and power (CHP) applications is investigated by a series of computer simulations. Natural gas is converted into hydrogen either by the combined oxidation–steam reforming, i.e. indirect partial oxidation mechanism on Pt-Ni catalyst or by the direct, one-step partial oxidation mechanism on Pt monoliths. A water–gas shift converter and a catalytic selective carbon monoxide oxidation unit are used for reducing carbon monoxide levels to a value which the anode of proton exchange membrane fuel cell (PEMFC) can tolerate. Unconverted hydrocarbons and hydrogen rejected from the fuel cell are considered to be oxidized in a Pt catalyst packed afterburner in order to supply energy to the system. Reactor simulations based on available kinetic data together with energy integration calculations indicate direct partial oxidation to give higher hydrogen yields corresponding to increased electrical power outputs and elevated efficiencies. Indirect partial oxidation has the advantage of operating simplicity, since the direct route runs only at millisecond level residence times and high temperatures. In both mechanisms, water injection and energy integration are critical issues in adjusting product yields and in temperature control. The simulation outputs are compared and validated by the results based on the thermodynamics of the pertinent mechanism.

Keywords: Computer simulations; Fuel cells; Hydrogen production; Methane oxidation; Methane steam reforming; Partial oxidation

1. Introduction

The use of fuel cell technology offers significant improvements in clean and efficient power generation and is an important alternative to conventional techniques. Fuel cells with different features can be employed in various industries. Their utilization in mobile applications is of great interest since the latest internal combustion engine technology coupled with converters cannot completely eliminate emissions, while fuel cell powered electrically driven vehicles can run at zero-emission levels [1,2]. Apart from vehicular facilities, small-scale combined heat and power (CHP) generation based on fuel cells up to 250 kW seems to be another emerging market for stationary applications such as hospitals, computer data centers and residential use [2,3].

A variety of fuel cells operating with different fuels and electrolytes are under investigation, but the proton exchange membrane fuel cell (PEMFC) fuelled by hydrogen seems to be the most promising option for both vehicular and small-scale CHP facilities due to its compactness, modularity, high power density, energy efficiency and fast response [3,4]. PEMFC operation requires the continuous availability of hydrogen, whose storage, transportation and availability are the major problems that will be encountered when it is directly used as a fuel. Hence, attention has been focused on the conversion of more readily available hydrocarbon fuels to hydrogen.

Natural gas accounts for almost half the world's feedstock for hydrogen and has the lowest greenhouse effect in terms of carbon dioxide emissions [5]. Since it is mainly composed of methane, the number of hydrogen atoms per carbon atom is close to 4:1, which is greater than those of higher hydrocarbon fuels such as LPG and gasoline. Natural gas also has a price advantage compared to other fossil fuels.

In this study, the possible use of natural gas as a fuel for hydrogen generation in small-scale CHP applications is investigated quantitatively. For this purpose, a mathematical model is developed to describe the complete fuel processor-fuel cell operation involving the partial oxidation reactor, the water–gas shift (WGS) converter, the CO cleanup unit, the fuel cell (PEMFC) and the catalytic afterburner unit. This model, based on kinetic data available in the literature, is used to simulate operations specialized for two different natural gas conversion mechanisms—

* Corresponding author. Tel.: +90-212-3581540x1875; fax: +90-212-2872460.
E-mail address: onsan@boun.edu.tr (Z.I. Önsan).

1385-8947/02/$ – see front matter
PII: S1385-8947(02)00069-4

Nomenclature

$c_{p,i}$	gas-phase heat capacity of i (kJ kmol^{-1} K^{-1})
c_{p_L,H_2O}	liquid phase heat capacity of water (kJ kmol^{-1} K^{-1})
$F_{CH_4^-}$	molar flow rate of unconverted methane (kmol h^{-1})
$F_{H_2^-}$	molar flow rate of hydrogen rejected from the fuel cell (kmol h^{-1})
F_{H_2O+}	molar flow rate of liquid water injected (kmol h^{-1})
F_i	molar flow rate of i (kmol h^{-1})
$F_{i,ex}$	molar flow rate of i at the reactor exit (kmol h^{-1})
$F_{i,exab}$	molar flow rate of i at the afterburner exit (kmol h^{-1})
F_{i,H_2ox}	molar flow rate of i after hydrogen oxidation within the afterburner (kmol h^{-1})
$F_{i,j}$	molar flow rate of i consumed in reaction j (kmol h^{-1})
$F_{i,ox}$	molar flow rate of i after total methane oxidation within the partial oxidation reactor (kmol h^{-1})
h	fraction of the recovered sensible heat from the partial oxidation reactor exit stream
h_{exab}	fraction of the recovered sensible heat from the afterburner exit stream
k_j	specific reaction rate of reaction j
$K_{P,j}$	equilibrium constant for reaction j
K_i'	adsorption/desorption equilibrium constant for i (atm^{-1})
P_i	partial pressure of i (atm)
q	heat input-removal terms in the energy balance equations (kJ)
$-r_j$	rate of reaction j (kmol kgcat^{-1} h^{-1})
R	gas constant (kJ kmol^{-1} K^{-1})
T	temperature of the gas mixture (K)
T_{ex}	temperature of the gas mixture at the partial oxidation reactor exit (K)
T_{ex+}	temperature of the gas mixture after the sensible heat recovery (K)
T_{exab}	temperature of the gas mixture at the afterburner exit (K)
T_f	final temperature of the gas mixture after ethane or propane oxidation (K)
$T_{H_2O}^{vap}$	vaporization temperature of water (K)
T_{LO}	light-off temperature of methane (K)
T_{max}	maximum catalyst bed temperature within the partial oxidation reactor (K)
W	catalyst weight (kg)

Greek letters

$\Delta H_{H_2O}^{vap}$	heat of vaporization of water (kJ kmol^{-1})
ΔH_j	molar enthalpy of reaction j (kJ kmol^{-1})
$\Delta H_{j,T}$	molar enthalpy of reaction j at temperature T (kJ kmol^{-1})
ν_{ji}	stoichiometric coefficient of i in reaction j
θ	empirical constant

Superscripts

$^\circ$	standard conditions
vap	vaporization

Subscripts

ex	partial oxidation reactor exit
exab	afterburner exit
f	final
i	component index
j	reaction number
LO	light-off
max	maximum

combined total oxidation (TOX)–steam reforming (SR), i.e. indirect partial oxidation, and direct partial oxidation. The results, validated by their thermodynamics-based counterparts, are expressed in terms of product yields as functions of water/fuel and fuel/oxygen ratios at the inlet. The comparison of the two operations is based on their product yields, their electrical power output efficiencies and their operating characteristics.

2. Process considerations

2.1. Hydrogen production in fuel processing unit

2.1.1. Indirect partial oxidation

Methane, which is considered as the model hydrocarbon for natural gas, can be converted to hydrogen on a bimetallic Pt-Ni catalyst [6] by indirect partial oxidation, which is a combination of TOX, SR and WGS reactions:

$$CH_4 + 2O_2 = CO_2 + 2H_2O, \quad \Delta H_1^\circ = -802.3\,\text{kJ/mol} \tag{1}$$

$$CH_4 + H_2O = CO + 3H_2, \qquad \Delta H_2^\circ = 206.2\,\text{kJ/mol} \tag{2}$$

$$CO + H_2O = CO_2 + H_2, \qquad \Delta H_3^\circ = -41.2\,\text{kJ/mol} \tag{3}$$

This operation, running in an adiabatically operating fixed-bed reactor, is autothermal in character, i.e. heat and part of the steam required by the endothermic SR is supplied by the exothermic TOX. The catalyst, Pt-Ni/δ-Al_2O_3, can safely operate at temperatures up to 1100 K, above which thermal sintering is significant. Careful control of the bed temperature is therefore required to prevent catalyst deactivation due to sintering. In addition, coke formation is likely to occur under SR conditions by several mechanisms [7], but it can be eliminated by keeping the steam/carbon ratio around 2.5 [8]. This ratio is different from the water/methane ratio which is related with the water and methane at the system inlet. The effect of TOX is taken into account in the steam/carbon ratio, which is defined as follows:

$$\text{steam/carbon ratio} = \frac{\text{moles of water fed} + \text{moles of water produced by TOX}}{\text{moles of methane fed} - \text{moles of methane consumed in TOX}} \tag{4}$$

Steam produced by TOX is usually not sufficient to meet the above requirements, and additional water should be fed into the partial oxidation reactor (Fig. 1) to control the catalyst bed temperature and to prevent carbon formation. This will also change the WGS equilibrium in the direction of increasing hydrogen yield and will remove an important portion of the carbon monoxide which significantly deactivates the Pt-based anode of the PEMFC. However, this reduction in CO content is usually insufficient, and the use of a WGS converter for further removal of CO is still required (Fig. 1).

Sulphur is present in natural gas in the form of simple compounds such as H_2S, COS, $(C_2H_5)_2S$, which are usually added to act as odorants [9]. However, their presence can affect SR in indirect partial oxidation as well as the operation of other catalytic units by reducing the lifetime of the pertinent catalysts [8,9]. In order to eliminate catalyst deactivation, a sulphur trap, packed with a mixture of cobalt and molybdenum oxides supported on alumina and ZnO particles [9], can be placed in front of the natural gas feed stream, as shown in Fig. 1. The use of sulphur-free natural gas is another solution which eliminates the requirement of a sulphur trap.

2.1.1.1. Light-off temperatures. Light-off temperature is defined as the value at which 10% of the oxidation conversion of a hydrocarbon is obtained [10]. In order to trigger the whole operation by initiating TOX, the catalyst bed temperature should be raised to the light-off value of the fuel of interest. This requires heat supply into the reactor, the amount of which is inversely proportional to the reactivity of the hydrocarbon. Methane is known to be a stable

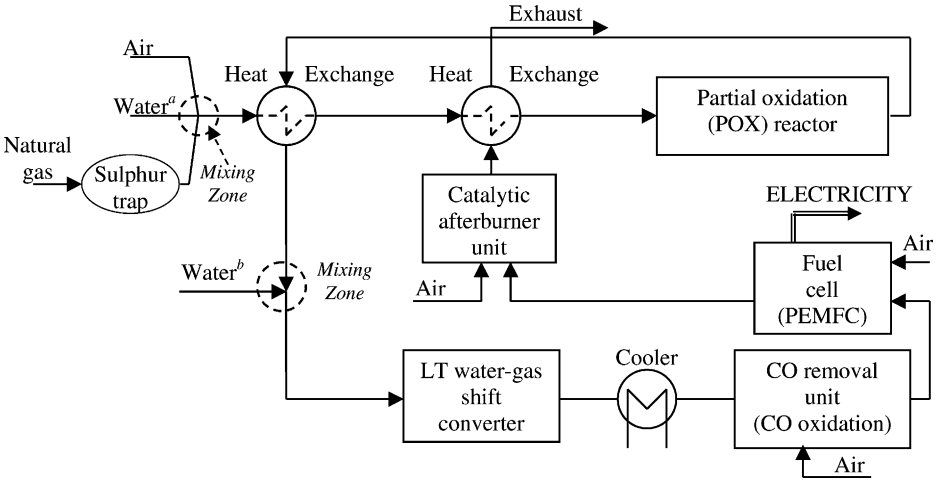

Fig. 1. Fuel processor/fuel cell operation (a) location of water injection in indirect partial oxidation; (b) location of water injection in direct partial oxidation.

molecule with light-off temperatures between 589 and 724 K depending on the hydrocarbon/air ratio [10]. However, natural gas also contains higher hydrocarbons such as ethane and propane, which start oxidizing at temperatures around 480–515 K and 425–458 K, respectively [10]:

$$C_2H_6 + 3.5O_2 = 2CO_2 + 3H_2O, \quad \Delta H_5^\circ = -1427.8\,\text{kJ/mol} \tag{5}$$

$$C_3H_8 + 5O_2 = 3CO_2 + 4H_2O, \quad \Delta H_6^\circ = -2044.0\,\text{kJ/mol} \tag{6}$$

The relative amounts of ethane and propane in natural gas are regionally dependent [11], but their presence ensures a lower energy requirement and earlier initiation of oxidation, which then helps in providing heat to sustain methane oxidation.

2.1.2. Direct partial oxidation

An alternative route for catalytic hydrogen production is direct partial oxidation (dry oxidation) and can be represented by the following reaction:

$$CH_4 + \tfrac{1}{2}O_2 = CO + 2H_2, \qquad \Delta H_7^\circ = -35.7\,\text{kJ/mol} \tag{7}$$

Schmidt and co-workers [12] reported 80% methane conversion on Pt-monoliths at temperatures around 1373 K and at contact times between 10^{-4} and 10^{-2} s. Thus, in contrast to indirect oxidation, mass transfer limitations are much more significant than kinetics in the direct conversion of methane [12]. These operating conditions do not allow SR, WGS and carbon formation mechanisms, which require much higher residence times to run.

In order to make use of the WGS reaction, a separate WGS converter is placed after the partial oxidation reactor, as shown in Fig. 1. In this operation, water is injected at the reactor exit, just after the sensible heat recovery of the hot exit gas stream and before the WGS converter (Fig. 1). Water addition adjusts the WGS equilibrium to reduce the CO level to values suitable for the operation of the CO removal unit and to increase the H_2 yield. Moreover, water injection further cools down the gas stream after heat recovery and satisfies the low temperature requirements of the shift converter, CO removal unit and the PEMFC.

2.2. Water–gas shift converter

The WGS converter is a separate fixed-bed reactor placed after the hydrogen generator in order to remove CO from the H_2-rich stream. It is packed with Cu/ZnO catalyst and operates at relatively low temperatures around 473 K. In indirect partial oxidation, WGS runs simultaneously with methane SR and removes most of the CO produced by the latter reaction. In dry oxidation, however, CO is a major product, but can be removed significantly in a single shift conversion when sufficient quantities of water are supplied. Moreover, energy integration allows temperature reduction down to low-temperature shift ranges (ca. 473 K). Therefore, another high temperature shift converter is not required in either operation.

The WGS reaction is slightly exothermic and results in temperature elevations. Therefore, a cooler is employed in order to reduce the shift converter exit temperatures down to the operating ranges of the selective CO oxidation unit and the PEMFC.

2.3. CO removal unit

CO is a poison for the anode catalyst of the PEMFC, since it strongly chemisorbs onto Pt and deactivates the catalyst for the anode reaction (H_2 oxidation). The Pt-based anode catalyst can tolerate a maximum of 40 ppm CO [13], which cannot be achieved by a single WGS converter. Hence, the CO concentration within the hydrogen rich stream should further be reduced by a separate operation. Moreover, this removal operation should work efficiently at low temperatures, since the PEMFC operates at a temperature range of 333–363 K.

Several methods such as selective oxidation of CO to CO_2, methanation of CO and the use of hydrogen diffusion membranes are proposed to meet the above-mentioned criteria [3,14]. During methanation, CO_2 may be converted along with CO, resulting in considerable H_2 loss. The use of Pd-based membranes requires high-pressure differentials and high temperatures both of which can significantly reduce the overall efficiency. All these factors make the selective oxidation method the optimal option for CO removal.

Trimm and Önsan [14] have reported the details of selective CO oxidation at low temperatures, indicating a precious metal based catalyst such as Pt to exhibit optimal performance.

2.4. Fuel cell and afterburner unit

The PEMFC is the unit producing the desired electrical power by converting the chemical energy stored within hydrogen into electricity. The PEMFC operation is represented by the following reactions occurring on the Pt-based cathode and anode at temperatures between 333 and 363 K [3]:

$$\text{anode reaction}: \quad H_2 = 2H^+ + 2e^- \tag{8}$$

$$\text{cathode reaction}: \quad \tfrac{1}{2}O_2 + 2H^+ + 2e^- = H_2O \tag{9}$$

The PEMFC rejects about 25% of the hydrogen that is fed into it [13]. There is also some unconverted methane within the gas mixture. These components—hydrogen and methane—are oxidized in a separate, adiabatic afterburner unit packed with a Pt-based catalyst to enable energy recovery within the entire system and to exhaust a clean gas free of hydrocarbons (Fig. 1):

$$H_2 + \tfrac{1}{2}O_2 = H_2O, \qquad \Delta H_{10}^\circ = -241.8\,\text{kJ/mol} \tag{10}$$

$$CH_4 + 2O_2 = CO_2 + 2H_2O, \qquad \Delta H_1^\circ = -802.3\,\text{kJ/mol}$$

Part of the sensible heat of the hot afterburner effluent stream is then recovered for providing additional energy to the feed stream in order to trigger the partial oxidation conversion (Fig. 1).

2.5. Energy integration

In both indirect and direct partial oxidation mechanisms, heat is required to overcome the low reactivity of methane, to evaporate the extra liquid water fed into the system and to sustain the H_2-generating reactions (reactions 2 and 7). On the other hand, the PEMFC, and hence, the CO removal unit and the WGS converter operate at relatively low temperatures. Hence, energy integration becomes vital for optimizing these operations.

One energy source is the high sensible heat of the partial oxidation reactor exit stream, which can be recovered either by heat exchange with the cold inlet stream or by water injection, as proposed in the direct route (Fig. 1). Such energy recovery also helps in reducing the temperature of the gas mixture to the fuel cell operating ranges. The hot exit stream from the catalytic afterburner is another energy source that contributes to the overall heat recovery of the operation (Fig. 1).

3. Modeling and simulation of hydrogen production

In order to evaluate the product yields as functions of water/methane and methane/oxygen ratios, computational algorithms specific for the two partial oxidation mechanisms are developed. In these algorithms, the aforementioned process considerations are taken into account in the light of the reaction kinetics. A methane feed of 1 kmol h^{-1} is taken as basis in both systems.

3.1. Indirect partial oxidation

The iterative algorithm developed for indirect partial oxidation assumes that both the partial oxidation reactor and the WGS converter operate adiabatically:

(a) TOX (reaction 1) is very fast compared with SR (reaction 2) and WGS (reaction 3). Its effect is dictated by the degree of conversion achieved. Hence, a conversion value is assumed for the TOX. The methane/oxygen ratios in the feed should be above the stoichiometric value (0.5) in order to leave some methane for SR.

(b) A value is assumed for the amount of water fed into the reactor, thus specifying the molar water/methane ratio at the inlet.

(c) The product distribution at the reactor exit is calculated by integrating the differential mole and energy balance equations along 1 kg of catalyst weight and solving the WGS equilibrium simultaneously, since the WGS reaction is fast and catalyzed by Ni to equilibrium [8]. The balance equations and the WGS equilibrium in the indirect partial oxidation unit are expressed as follows:

$$\frac{\mathrm{d}F_i}{\mathrm{d}W} = \sum_j (\nu_{ji})(-r_{ji}) \tag{11}$$

$$\frac{\mathrm{d}T}{\mathrm{d}W} = \frac{\sum_j (-\Delta H_j)(-r_j)}{\sum_i F_i c_{p,i}} \tag{12}$$

$$\text{At } W = 0, \quad F_i = F_{i,\mathrm{ox}}, T = T_{\max} \tag{13}$$

$$K_{P,3} = \frac{P_{\mathrm{CO_2}} P_{\mathrm{H_2}}}{P_{\mathrm{CO}} P_{\mathrm{H_2O}}} \tag{14}$$

The kinetics of the methane SR is represented by the rate expression proposed by Ma et. al [15]:

$$-r_2 = \frac{k_2 P_{\mathrm{CH_4}}^{0.96} P_{\mathrm{H_2O}}^{-0.17}}{1 + \theta P_{\mathrm{H_2}}^{0.25}} \tag{15}$$

It is worth noting that the SR reaction running on a Pt-Ni catalyst is much faster on Ni than on Pt [10,15]. Hence, Eq. (15), derived for Ni catalyzed reforming, is taken to be sufficiently effective in simulating the indirect conversion route.

(d) The product distribution at the exit of the shift converter is determined using the following model equations integrated along 0.5 kg catalyst together with the rate expression describing the kinetics of the WGS reaction on Cu/ZnO [16]:

$$\frac{\mathrm{d}F_i}{\mathrm{d}W} = (\nu_{3i})(-r_{3i}) \tag{16}$$

$$\frac{\mathrm{d}T}{\mathrm{d}W} = \frac{(-\Delta H_3)(-r_3)}{\sum_i F_i c_{p,i}} \tag{17}$$

$$\text{At } W = 0, F_i = F_{i,\mathrm{ex}}, T = 473\,\mathrm{K} \tag{18}$$

$$-r_3 = \frac{k_3 P_{\mathrm{CO}} P_{\mathrm{H_2O}} [1 - (P_{\mathrm{CO_2}} P_{\mathrm{H_2}})/(P_{\mathrm{CO}} P_{\mathrm{H_2O}} K_{P,3})]}{(1 + K'_{\mathrm{CO}} P_{\mathrm{CO}} + K'_{\mathrm{H_2O}} P_{\mathrm{H_2O}} + K'_{\mathrm{CO_2}} P_{\mathrm{CO_2}} + K'_{\mathrm{H_2}} P_{\mathrm{H_2}})^2} \tag{19}$$

(e) The temperature at the exit of the catalytic afterburner, T_{exab}, is calculated from the following energy balance:

$$q_{1,1} = F_{\mathrm{H_2^-}} \Delta H_{10,353} \tag{20}$$

$$q_{1,2} = F_{\mathrm{CH_4^-}} \Delta H_{1,T_{\mathrm{LO}}} \tag{21}$$

$$q_{1,3} = \sum_i F_{i,\mathrm{H_2ox}} \int_{353}^{T_{\mathrm{LO}}} c_{p,i}\,\mathrm{d}T \tag{22}$$

$$q_{1,4} = \sum_i F_{i,\mathrm{exab}} \int_{298}^{T_{\mathrm{exab}}} c_{p,i}\,\mathrm{d}T \tag{23}$$

$$\sum_{k=1}^{4} q_{1,k} = 0 \tag{24}$$

The exit temperature from the PEMFC, which is taken to be 353 K, is considered as the inlet temperature to the afterburner unit. In Eqs. (20)–(23), $q_{1,1}$ and $q_{1,2}$ are the quantities of heat released by the total combustion of hydrogen and methane, respectively. Hydrogen is easily oxidized, but the temperature of the gas mixture should be raised to the light-off value of methane ($T_{LO} = 589$ K, [10]) for its combustion. The quantity of heat required for this purpose is represented by $q_{1,3}$ within the energy balance given in Eq. (22). Finally, $q_{1,4}$ corresponds to the sensible heat of the gas mixture at the afterburner exit.

(f) The amount of injected water assumed in step (b) is checked by solving the energy balance around the partial oxidation reactor given in Eq. (32) for the maximum catalyst bed temperature, T_{max}:

$$q_{2,1} = F_{CH_4,2}\Delta H_{2,T_{max}} \quad (25)$$

$$q_{2,2} = F_{H_2O+}(c_{p_L,H_2O}(T^{vap}_{H_2O} - 298) + \Delta H^{vap}_{H_2O}) \quad (26)$$

$$q_{2,3} = \sum_i (F_{i,ox}) \int_{T_{LO}}^{T_{max}} c_{p,i}\, dT \quad (27)$$

$$q_{2,4} = F_{CH_4,1}\Delta H_{1,T_{LO}} \quad (28)$$

$$q_{2,5} = -h \sum_i (F_{i,ex}) \int_{298}^{T_{ex}} c_{p,i}\, dT \quad (29)$$

$$q_{2,6} = -h_{exab} \sum_i (F_{i,exab}) \int_{298}^{T_{exab}} c_{p,i}\, dT \quad (30)$$

$$q_{2,7} = F_{CO,3}\Delta H_{3,T_{ex}} \quad (31)$$

$$\sum_{k=1}^{7} q_{2,k} = 0 \quad (32)$$

In Eqs. (25)–(31), $q_{2,1}$ is the amount of heat required by SR, $q_{2,2}$ is the amount of heat required for evaporating the injected water, $q_{2,3}$ is the amount of the energy used by the reaction mixture for temperature rise after TOX from T_{LO} to T_{max}, $q_{2,4}$ is the amount of heat released by TOX, $q_{2,5}$ and $q_{2,6}$ are the amounts of sensible heat recovered from the reactor and afterburner exit streams, respectively, and finally, $q_{2,7}$ is the amount of heat released by the WGS reaction. In the simulations, the sensible heat recovery levels from the reactor and afterburner exit streams are assumed to be 70%, i.e. the coefficients h and h_{exab} in Eqs. (29) and (30), respectively are taken to be equal to 0.7.

(g) Steps (b–f) are repeated until the amount of water fed into the reactor, i.e. water/methane ratio, satisfying the maximum bed temperature criterion ($T_{max} = 1100 \pm 10$ K) is obtained.

(h) The algorithm above is repeated for different values of the TOX conversions to obtain product yields as functions of methane/oxygen and water/methane ratios.

3.2. Direct partial oxidation

Since the kinetics of reaction (7) is fast, and external mass transport resistances control the degree of product yield, the reactor conditions and conversion values reported for the direct oxidation of methane [12] are employed in the algorithm below:

(a) The temperature at the reactor exit, T_{ex}, is calculated from the following energy balance:

$$F_{CH_4,7}\,\Delta H_{7,1373} = \sum_i (F_{i,ex}) \int_{1373}^{T_{ex}} c_{p,i}\, dT \quad (33)$$

(b) A value between 0.1 and 0.85 is assumed for the sensible heat recovery from the reactor exit stream, h. The temperature of the gas stream after the specified heat recovery, T_{ex+}, is calculated by solving the following energy balance:

$$(1-h)\sum_i (F_{i,ex}) \int_{298}^{T_{ex}} c_{p,i}\, dT = \sum_i (F_{i,ex}) \int_{298}^{T_{ex+}} c_{p,i}\, dT \quad (34)$$

(c) The inlet temperature to the low temperature WGS converter is taken to be 473 K. Then, the amount of water needed for reducing the temperature of the gas mixture to 473 K, F_{H_2O+}, is evaluated using the energy balance given in Eq. (37):

$$q_{3,1} = F_{H_2O+}(c_{p_L,H_2O}(T^{vap}_{H_2O} - 298) + \Delta H^{vap}_{H_2O}) \quad (35)$$

$$q_{3,2} = \sum_i (F_{i,ex}) \int_{T_{ex+}}^{473} c_{p,i}\, dT \quad (36)$$

$$\sum_{k=1}^{2} q_{3,k} = 0 \quad (37)$$

In Eqs. (35) and (36), $q_{3,1}$ is the amount of heat required to vaporize the injected water and $q_{3,2}$ is the amount of energy lost from the gas stream after the water injection, which will result in a final temperature of 473 K. Note that part of the sensible heat of the reactor exit stream is recovered previously in step (b).

(d) The product distribution at the exit of the shift converter is determined as explained in step (d) of the indirect partial oxidation algorithm.

(e) The temperature at the afterburner exit is calculated as explained in step (e) of the indirect partial oxidation algorithm.

(f) Steps (b–e) are repeated for different values of the sensible heat recovery to obtain product yields as a function of water/methane ratio. It is worth noting that the methane/oxygen ratio at the inlet is fixed at the stoichiometric value for reaction (7) [12].

3.3. Thermodynamic predictions

In order to check whether the results based on kinetic data are within thermodynamic limits, the simulations are repeated using the same algorithms above with the following differences in respective steps:

- In indirect partial oxidation, a temperature rise occurs after methane light-off due to the high exothermicity of the methane oxidation. The maximum allowable bed temperature is 1100 K, which is controlled by water injection into the reactor. SR, which runs after TOX, is endothermic, leading to a decrease in the bed temperature. The hydrogen-rich effluent, whose composition is dictated by SR and WGS equilibria [8,17], leaves the reactor at a lower temperature. Therefore, solving methane SR and WGS equilibria simultaneously at reactor exit conditions (850 K, 1.5 atm) gives the product distribution at the reactor effluent stream:

$$K_{P,2} = \frac{P_{CO} P_{H_2}^3}{P_{CH_4} P_{H_2O}} \tag{38}$$

$$K_{P,3} = \frac{P_{CO_2} P_{H_2}}{P_{CO} P_{H_2O}} \tag{14}$$

  Similarly, the product composition at the WGS converter exit is determined by solving Eq. (14) at 473 K.
- Due to the dominance of mass transfer effects over kinetics [12] in direct partial oxidation, the reactor operation is considered to be the same as described in Section 3.2. The major difference is the use of Eq. (14) instead of Eqs. (16)–(18) for calculating the product yields at the exit of the shift converter.

3.4. Effects of ethane and propane in natural gas

Ethane and propane, which are more reactive than methane, contribute to the energy input of the operation by their easier and earlier oxidation. This phenomenon, i.e. temperature rises due to reactions (5) and (6) can be quantified using the energy balance equations given below for ethane and propane, respectively:

$$F_{C_2H_{6,5}} \Delta H_{5,480} = \sum_i (F_{i,ox}) \int_{480}^{T_f} c_{p,i} \, dT \tag{39}$$

$$F_{C_3H_{8,6}} \Delta H_{6,425} = \sum_i (F_{i,ox}) \int_{425}^{T_f} c_{p,i} \, dT \tag{40}$$

3.5. Numerical solution techniques

The equilibrium expressions, Eqs. (14) and (38), and the energy balances, Eqs. (24), (32)-(34), (37), (39) and (40), are nonlinear algebraic equations in character. A Gauss–Newton based optimization routine is employed for their mathematical solution. The differential mole and energy balances, Eqs. (11) and (12) and the WGS equilibrium, Eq. (14), form a differential–algebraic equation set to be solved simultaneously. For this purpose, a variable order, stiff ordinary differential equation (ODE) solver based on numerical differentiation formulas and the Gauss–Newton based algebraic equation solver are employed interactively. The same ODE solver is used in integrating the differential set of Eqs. (16) and (17). The computer codes are prepared using the MATLAB^{TM} environment and executed using an IBM Netfinity M10 workstation.

4. Results and discussion

The simulation results of the indirect and the direct partial oxidation of methane are given in Figs. 2 and 3, respectively, and expressed in terms of product yields defined as the number of moles of product obtained per mole of methane fed into the system. The effects of water/methane and methane/oxygen ratios at the inlet and of sensible heat recovery levels on the product yields are indicated on the pertinent plots.

4.1. Water injection

It was previously mentioned that the steam/carbon ratio defined in Eq. (4) should be kept above 2.5 to eliminate carbon formation in the oxidation/SR case [8]. Table 1 demonstrates the values of TOX conversions, corresponding methane/oxygen and steam/carbon ratios obtained without water injection. The maximum value of the steam/carbon ratio is found to be 1.77, indicating the requirement for an external water supply into the system. It is worth noting that the steam produced by TOX would be sufficient if a precious metal catalyst such as Rh, which allows much less coke formation in reforming, was used instead of Ni [14,18].

The selective oxidation unit can successfully reduce the CO content down to 40 ppm, when a gas mixture with a CO composition below 2 mol% is fed into it [13]. In the direct oxidation route where methane conversion is taken to

Table 1
TOX conversion levels and related methane/air and steam/carbon ratios leading to converged solutions in thermodynamically and kinetically controlled cases in indirect partial oxidation

Kinetics			Thermodynamics		
TOX conversion	CH_4/air	Steam/carbon	TOX conversion	CH_4/air	Steam/carbon
0.25	0.53	0.67	0.10	1.33	0.22
0.27	0.49	0.74	0.13	1.02	0.30
0.31	0.43	0.90	0.16	0.83	0.38
0.33	0.40	0.99	0.20	0.66	0.50
0.36	0.37	1.13	0.25	0.53	0.67
0.47	0.28	1.77	0.30	0.44	0.86
–	–	–	0.35	0.38	1.08

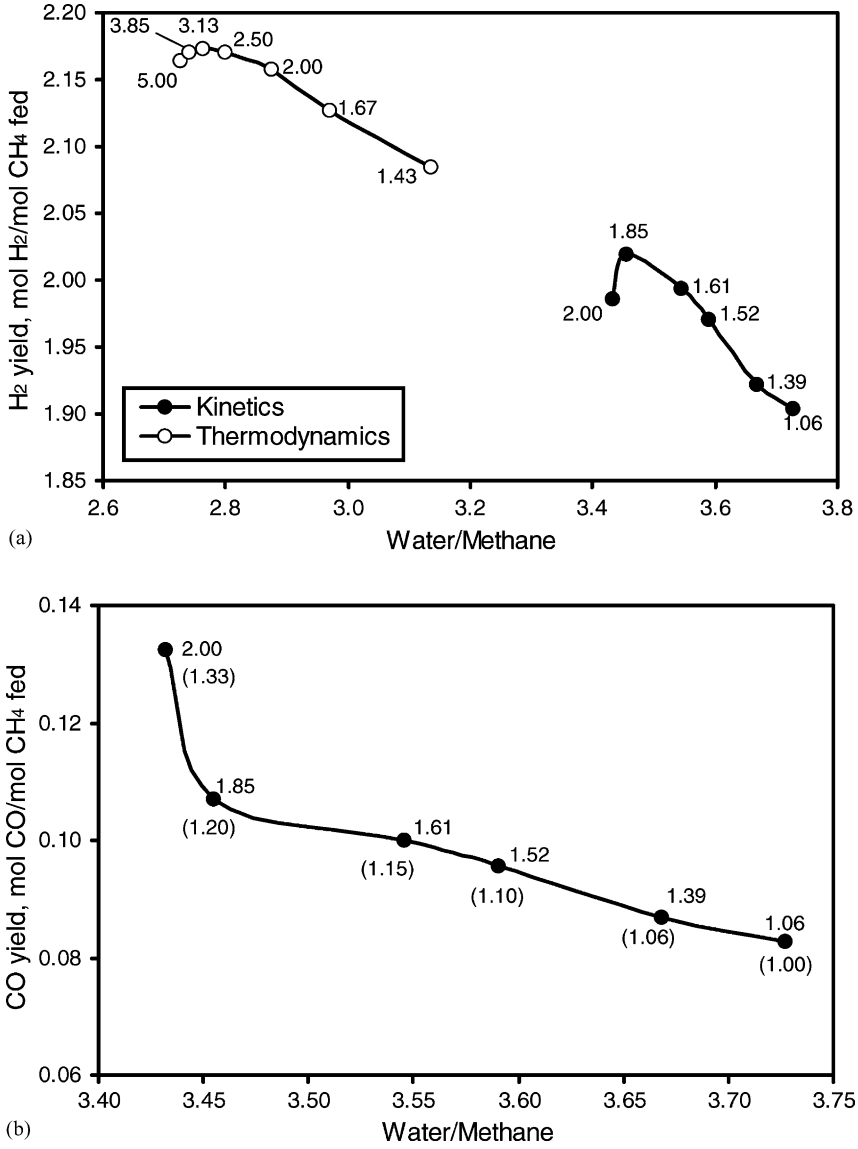

Fig. 2. (a) Effects of methane/oxygen (shown within the figure), and water/methane ratios at the system inlet on H_2 yield (moles of H_2 produced/mole of methane fed) in indirect partial oxidation of methane, (b) effects of methane/oxygen (shown within the figure), and water/methane ratios at the system inlet on CO yield (moles of CO produced/mole of methane fed) in indirect partial oxidation of methane (molar percentage of CO within the gas mixture is shown within the figure in parenthesis).

be 80% [12], the mole fraction of CO at the reactor exit is equal to ca. 0.2, which is ten times greater than the value that the CO cleanup unit can tolerate (0.02). Therefore, external water injection is required to eliminate coke formation and to drive the WGS reaction for reducing CO levels in indirect and direct conversion routes, respectively.

4.2. Product yields

Both thermodynamics and kinetics based H_2 yields obtained in indirect partial oxidation are found to have maximum values at certain water/methane and methane/oxygen ratios (Fig. 2a). SR is endothermic and gives higher hydrogen yields at high temperatures generated by the TOX. The more the methane is oxidized at lower methane/oxygen ratios, the higher the bed temperatures. However, this leads to lower amounts of methane reserved for SR, meaning lower hydrogen yields. In the opposite case, where more methane is reserved for reforming, hydrogen production is expected to be lower, since oxidation is limited and bed temperature may not be adequate to drive SR due to higher methane/oxygen ratios. This characteristic feature of the indirect partial oxidation leads to the existence of maxima in hydrogen yields.

In contrast with the indirect route, H_2 yields given in Fig. 3a for direct oxidation seem to flatten at their maximum values. H_2 yields obtained in direct oxidation depend on the degree of sensible heat recovery, h, at the reactor exit, and hence, on the amount of water injected to

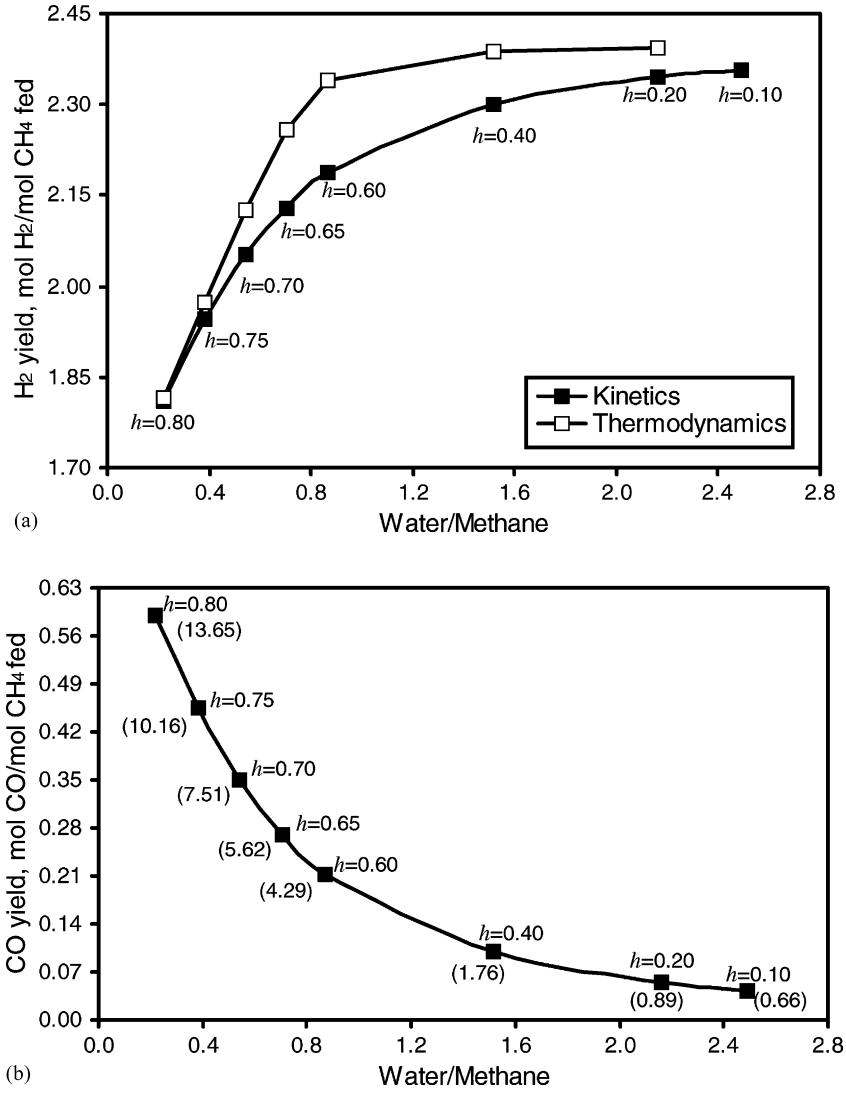

Fig. 3. (a) Effects of sensible heat recovery, h (shown within the figure), and water/methane ratio at the system inlet on H_2 yield (moles of H_2 produced/mole of methane fed) in direct partial oxidation of methane, (b) effects of sensible heat recovery, h (shown within the figure), and water/methane ratio at the system inlet on CO yield (moles of CO produced/mole of methane fed) in direct partial oxidation of methane (molar percentage of CO within the gas mixture is shown within the figure in parenthesis).

cool the gas mixture for the shift conversion (Fig. 1). The higher the heat recovery, the lower the amount of water that needs to be injected. Therefore, at higher values of h, i.e. lower water/methane ratios, water will be the limiting reactant and H_2 yields will increase with increasing quantities of water (Fig. 3a). However, as the heat recovery decreases, CO becomes the limiting reactant after certain water/methane ratios (0.85 in thermodynamic case, 2.15 in kinetic case), and H_2 yields reach their maximum value and remain almost constant, since the amount of CO generated by the direct oxidation reaction is fixed (Fig. 3a). This reasoning is also valid for the trend of CO yields given in Fig. 3b.

In both indirect and direct partial oxidation, the amounts of CO decrease with increasing water/methane ratios (Figs. 2b and 3b). The WGS reaction, driven by the externally injected water to a great extent, is considered as the major factor that reduces the CO yields.

4.3. Direct partial oxidation versus indirect partial oxidation

The comparison of the two operations is based on product yields obtained in the kinetically controlled cases, as well as their electrical power production efficiencies, which is defined as follows:

$$\text{efficiency} = \frac{\text{actual PEMFC power obtained in kW}}{\text{theoretical PEMFC output in kW}} \times 100 \quad (41)$$

The theoretical PEMFC power in the denominator is dictated by the maximum amount of hydrogen that could be

expected from indirect and direct partial oxidation routes, which are 4 mol of hydrogen via reactions 2 and 3, and 3 mol of hydrogen via reactions 3 and 7, respectively. However, only 75% of the hydrogen produced can be converted into electrical power, since the PEMFC rejects ca. 25% of the hydrogen fed into it [13]. Therefore, the theoretical output would correspond to 87 and 65 kW power for oxidation/SR and direct oxidation routes, respectively, assuming that 1000 l H_2 h^{-1} would correspond to 1 kW electrical power [13], the PEMFC operates at 353 K and that 1 kmol h^{-1} of methane is fed into both systems.

An important point should be highlighted for the direct conversion route. It was mentioned that the selective CO oxidation unit, which reduces the CO levels to less than 40 ppm for the PEMFC operation, accepts a gas mixture with CO content below 2 mol% [13]. This condition, corresponding to a CO yield of ca. 0.1 mol CO/mol CH_4, is only valid above a water/methane ratio of 1.45 (Fig. 3b). In other words, the actual operating region for direct partial oxidation is determined by water/methane ratios greater than 1.45.

The actual maximum H_2 yield obtained in the direct conversion mechanism (2.36 mol H_2/mol CH_4) at a water/methane ratio of 2.49 is found to be higher than that estimated for the indirect partial oxidation (2.02 mol H_2/mol CH_4) at a water/methane ratio of 3.45 (Figs. 2a and 3a). These H_2 yields are equivalent to 51 and 44 kW power output, respectively, and corresponding to 78% efficiency for direct oxidation and 51% efficiency for oxidation/SR. Although the theoretical power output is higher in the indirect scheme, the direct route seems to be better in terms of higher H_2 yields and hence improved electrical power production efficiencies. The improved conversion of methane in direct oxidation (ca. 80% at 1373 K [12]) and the conversion of most of the CO formed in reaction 7 to H_2 in the WGS converter via reaction 3 lead to hydrogen quantities higher than those obtained in the indirect oxidation route in which approximately 28% of the methane fed is lost during TOX and conversion of remaining methane during SR is found to be reported at around 70% [14]. The WGS effect, i.e. conversion of the resulting CO into H_2, exercised both in the indirect partial oxidation reactor and in the shift converter is insufficient in reaching H_2 yields achieved in the direct route.

The CO yield and the corresponding molar CO composition are found to be 0.11 mol CO/mol CH_4 and 1.2 mol% of CO, respectively at a water/methane ratio of 3.45 in indirect partial oxidation (Fig. 2b). These figures are equivalent to 0.04 mol CO/mol CH_4 and 0.66 mol% of CO at a water/methane ratio of 2.49 in direct partial oxidation followed by WGS conversion (Fig. 3b). These results indicate that the direct route gives lower amounts of CO, requiring reduced quantities of selective oxidation catalyst and hence a more compact CO cleanup unit.

Although the direct partial oxidation method seems to be promising in terms of the efficiency defined in Eq. (41) and in terms of CO yields, it has serious operational challenges such as the requirement of high gas flow rates corresponding to millisecond-level contact times, high operating temperatures and the presence of near-explosive conditions [12] that have to be overcome. These features are much more pronounced during transient periods such as start up and shut down operations which are exercised much less frequently in residential CHP facilities. The direct route may therefore be a promising fuel processing option for stationary applications. It is also worth noting that, a specific catalyst—Ru supported on TiO_2—is reported to exhibit an exceptional behavior in terms of catalyzing direct partial oxidation at relatively lower temperatures (ca. 973–1073 K) and at longer contact times [19].

The latter mechanism is also preferable from an energetics point of view: it is found that a low sensible heat recovery of around 10% from the mixture at reactor exit, together with 30% heat recovery from the afterburner exit mixture, is sufficient to raise the temperature of the fuel and air feed stream (298 K) to 1373 K at which direct partial oxidation takes place. Therefore, higher levels of sensible heat and energy released from the afterburner can be used in applications such as central heating in addition to supplying electrical power.

4.4. Thermodynamics versus kinetics

Thermodynamics-based H_2 yields are presented together with their kinetics-based counterparts in Figs. 2a and 3a for indirect and direct partial oxidation mechanisms, respectively. In both operations, the results based on kinetics are within thermodynamic limit, as expected, verifying the kinetic data used in the simulations.

In order to drive the kinetics of the endothermic SR, a higher amount of energy is required. This leads to elevated TOX conversions in the kinetically controlled case, as shown in Table 1, and to higher heat evolution within the catalyst bed. Increased amounts of water are, therefore, injected into the system for controlling the bed temperature at 1100 K, resulting in greater water/methane ratios in the kinetics-based simulation results (Fig. 2).

4.5. Mobile applications

The ease of operation and carried weight are issues that are much more critical in mobile fuel cell applications. Although direct oxidation is better in terms of power output efficiency, simpler indirect partial oxidation route seems to be the operation of choice for fuel conversion in hydrogen driven fuel cell vehicles, since the latter is much more suitable for handling transient periods usually exercised in mobile applications. However, if coupled with a natural gas engine to drive the vehicle, the high-efficiency direct oxidation based route can be integrated with a fuel cell based auxiliary power unit (APU) to feed the peripherals within a vehicle. Natural gas engines have good efficiency, can follow driving dynamics and therefore can handle the

transient periods in vehicular operation. Electrical power demand for the peripherals is much less variable and can easily be provided by a fuel cell based APU integrated with a direct partial oxidation based hydrogen generation unit.

Although natural gas has the advantages of high H:C ratio and lowest CO_2 emissions, if used in vehicles, it will require heavy gas storage cylinders, resulting in increased carried weight and higher fuel consumption, and hence is not recommended. An extensive study about the use of alternative hydrocarbon fuels in vehicular fuel cell applications has previously been reported [20].

4.6. Ethane and propane in natural gas

In order to investigate the effects of ethane and propane on the energetics of the reactor operation, a hypothetical natural gas composition with 95 mol% methane and 5% ethane or propane and a feed with water/fuel ratio of 2.5 are considered. Solution of energy balances (39) and (40) gave temperature rises of 110 and 120 K in the gas mixture after oxidation of residual ethane and propane, respectively. These figures indicate that propane has a higher contribution to the energy input of the operation, since its molar heat of combustion (−2044 kJ) is greater than that of ethane (−1428 kJ). The resulting energy input quantified by these elevated temperatures leads to the easier oxidation of methane, requiring temperatures greater than 589 K [10].

5. Conclusions

The use of natural gas (modeled as methane) as a fuel for catalytic conversion to hydrogen in fuel processor-fuel cell systems for small-scale stationary CHP applications is investigated by a series of computer simulations. Two systems specialized for different fuel conversion operations—combined TOX–SR (indirect partial oxidation) and one step, dry oxidation (direct partial oxidation)—are of interest. In both systems, water injection is found to be necessary for product yield adjustment and temperature control. The indirect partial oxidation mechanism seems to be the operation of choice due to its practicality. The H_2 yields, calculated on the basis of kinetic data and verified by thermodynamics, are found to be higher in the direct oxidation route, leading to increased power outputs and efficiencies. The direct oxidation method, however, requires high temperatures, short contact times and near explosive conditions, but it may be exercised in stationary CHP applications in which start up and shut down are less frequent. Earlier oxidation of the ethane and/or propane present in natural gas increases the gas mixture temperature, which may help in the reduction of the energy demand for methane combustion.

Acknowledgements

Financial support provided by Boğaziçi University through project DPT-97K120640 is acknowledged.

References

[1] B.J. Cooper, Catalysis for the next decade, Platinum Metals Rev. 38 (1994) 2.
[2] P.G. Gray, M.I. Petch, Advances with HotSpot™ fuel processing, Platinum Metals Rev. 44 (2000) 108.
[3] T.R. Ralph, G.A. Hards, Powering the cars and homes of tomorrow, Chem. Ind. 9 (1998) 337.
[4] T.R. Ralph, Clean fuel cell energy for today, Platinum Metals Rev. 43 (1999) 14.
[5] J.N. Armor, The multiple roles of catalysis in the production of H_2, Appl. Catal. A 176 (1999) 159.
[6] L. Ma, D.L. Trimm, Alternative catalyst bed configurations for the autothermic conversion of methane to hydrogen, Appl. Catal. A 138 (1996) 265.
[7] D.L. Trimm, Catalysts for the control of coking during steam reforming, Catal. Today 49 (1999) 3.
[8] J.R. Rostrup-Nielsen, Catalytic steam reforming, in: J.R. Anderson, M. Boudart (Eds.), Catalysis, Science & Technology, Vol. 5, Springer, Berlin, 1984, pp. 1–117.
[9] L. Dicks, Hydrogen generation from natural gas for the fuel cell systems of tomorrow, J. Power Sources 61 (1996) 113.
[10] L. Ma, D.L. Trimm, C. Jiang, The design and testing of an autothermal reactor for the conversion of light hydrocarbons to hydrogen. 1. The kinetics of the catalytic oxidation of light hydrocarbons, Appl. Catal. A 138 (1996) 275.
[11] B. Tindall, D. King, Designing steam reformers for hydrogen production, Hydrocarbon Process. 73 (1994) 69.
[12] D.A. Hickman, L.D. Schmidt, Synthesis gas formation by direct oxidation of methane over Pt monoliths, J. Catal. 138 (1992) 267.
[13] S. Golunski, HotSpot™ fuel processor, Platinum Metals Rev. 42 (1998) 2.
[14] D.L. Trimm, Z.İ. Önsan, On board fuel conversion for hydrogen fuel cell driven vehicles, Catal. Rev. Sci. Eng. 43 (2001) 31.
[15] L. Ma, C.J. Jiang, A.A. Adesina, D.L. Trimm, Kinetic studies of steam reforming of light hydrocarbons over nickel based catalysts, in: Proceedings of the 22nd Australian and New Zealand Chemical Engineering Conference, CHEMECA 94, Vol. 1, Perth, 1994, p. 189.
[16] N.E. Amadeo, M.A. Laborde, Hydrogen production from the low-temperature water–gas shift reaction: kinetics and simulation of the industrial reactor, Int. J. Hydrogen Energy 20 (1995) 949.
[17] A.K. Avcı, D.L. Trimm, Z.I. Önsan, Heterogeneous reactor modeling for simulation of catalytic oxidation and steam reforming of methane, Chem. Eng. Sci. 56 (2001) 641.
[18] J.R. Rostrup-Nielsen, J.H. Bak Hansen, CO_2-reforming of methane over transition metals, J. Catal. 144 (1993) 38.
[19] C. Elmasides, T. Ioannides, X.E. Verykios, Kinetic model of the partial oxidation of methane to synthesis gas over Ru/TiO_2 catalyst, AIChE J. 46 (2000) 1260.
[20] A.K. Avcı, Z.I. Önsan, D.L. Trimm, On-board fuel conversion for hydrogen fuel cells: comparison of different fuels by computer simulations, Appl. Catal. A 216 (2001) 243.